COMPUTATIONAL FLUID DYNAMICS ANALYSIS FOR IMPROVING THE UNIFORMITY OF FLOW FIELD IN HEAT AIR DRYING KILNS

by

Yifeng ZHU[1,*], Liping SUN[1], Lifu WAN[1]

[1]*Northeast Forestry University, Harbin, Heilongjiang, China 150000*

**Corresponding author; E-mail: zhuyifeng@nefu.edu.cn*

Because the uniformity of the wind speed flow field in the hot air drying kiln directly affects the distribution of the temperature field in the kiln, to improve the uniformity of air distribution in the existing wood hot air drying kiln, CFD software was used to analyze the three-dimensional flow field of each improved scheme. A combination of visual comparison and analysis methods and data comparison and analysis methods be used, to serve as the basis for assessing the feasibility and rationality of the improvement schemes. Without adding baffle plates or altering the structure to incorporate right-angle surfaces, the kiln's structure was optimized by adjusting the position of the air outlet and installing airflow distribution chambers. This paper innovatively introduces the Theory of Inventive Problem Solving（TRIZ）to analyze and solve the flow field optimization problem in the kiln. The difference between this method and the existing research methods is that the solution process is more logical and the solution to the fundamental problem is more accurate. The experimental results show that when the air supply speed of scheme S_8 *is 3m/s~7m/s, the flow field of kiln Zone C (material drying area) meets the ideal range of 1m/s~3m/s. In addition, under the same working condition (3m/s), the velocity differences of scheme* S_8 *is closer to 0 than that of scheme* S_0*, and the velocity unevenness coefficient is reduced by 18.44%.*

Keywords: *hot air drying kiln, CFD, numerical simulation, wind speed flow field*

1. Introduction

Due to the low cost and wide applicability of hot air drying technology, it has become the research focus to improve the drying quality and drying efficiency of materials in the forestry field[1]. However, the high energy consumption and subpar quality resulting from the uneven distribution of airflow field within hot air drying devices have emerged as primary challenges that various drying apparatuses aim to address[2]. Because the uniformity of the flow field inside the kiln directly affects the temperature distribution inside the kiln[3,4], improving the uniformity of the internal flow field distribution in the hot air drying kiln is key to increasing the yield of dried materials, reducing drying time, and lowering energy consumption during the drying process.

Kadem S *et al.*[5] developed a 3-D comprehensive heat and mass transfer model for wood drying and conducted finite element analysis. Mecha P *et al.*[6] studied the optimal combinations of temperature (40~60 degrees Celsius) and air velocity (2m/s, 4m/s, and 6m/s) for drying machines. Marković Z. J *et al.*[7] analyzed the influence of plate position on airflow by numerical simulation of gas flow in porous plate rectangular channels. Chen Z.F *et al.*[8] improved the structure of inlet variable diameter angle pipes and verified the effectiveness of the improvement scheme in solving the problem of uneven airflow distribution in single-sided ventilation vertical box-type dryers using FLUENT software. Chen Z.J *et al.*[9] conducted simulations and optimizations of velocity and temperature field distributions in hot air drying chambers under different air supply parameters using computational fluid dynamics methods. Lan L.X *et al.*[10] conducted simulation and modeling of the internal flow field of the sedimentation separation device. They validated that the application of curved deceleration baffles can reduce the settling loss rate by obtaining airflow velocity contour maps and streamline maps. Wang Z.W *et al.*[11] achieved solutions to problems of product quality instability and low drying efficiency in heat pump drying chambers during the drying process by improving the chamber's structure and velocity parameters based on numerical simulations of airflow distribution inside the chamber. In all of these studies, Computational Fluid Dynamics (CFD) has been demonstrated as an effective numerical simulation tool for analyzing and improving thermal air-drying devices.

Wood drying, similar to drying other moist materials, is a comprehensive process of heat and mass transfer between the drying medium and the wood material[12]. This article takes a hot air drying kiln as an example, using sawn timber as the drying object. In response to the uneven distribution of the flow field inside the hot air drying kiln, without adding guide plates and without imposing constraints on right-angle structural curvature, the kiln structure is optimized and designed from two angles: changing the position of the air outlet and adding an airflow distribution chamber. Numerical simulations of the current and improved designs were conducted using the CFD software FLUENT. The CFD-Post processing software was used to output numerical simulation data of the flow field inside the kiln. Five evaluation indicators were formed by combining visual comparison and analysis methods (such as velocity contour maps and streamline maps) with data comparison and analysis methods (such as velocity differences, overall mean velocity distribution, and velocity unevenness coefficient). These indicators were used to compare and evaluate the effects of different kiln structural parameters on flow field characteristics after optimization, thus obtaining the optimal solution.

2. Model and Mathematical Formulation

2.1 Modelling and Initial Problem

A 3-D structural model of the single-sided hot air drying kiln was established using SpaceClaim software, as shown in Fig. 1(a). Based on the guiding effect of the kiln structure on the drying medium, the interior of the kiln is divided into four drying medium flow regions, a total of 15 monitoring points are arranged inside the kiln to collect flow velocity data of the drying medium, as shown in fig.1(b).

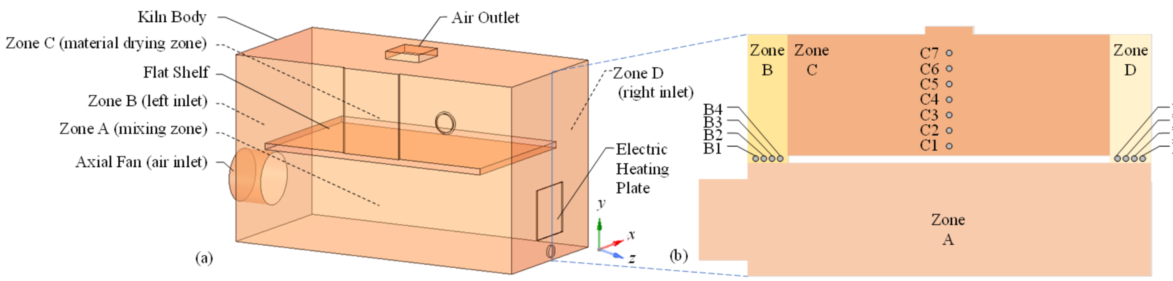

Figure 1. Single-sided hot air drying kiln; (a)3-D structure model, (b)Kiln partition situation and the distribution of detection points in the kiln

The main technical parameters of the hot air drying kiln are shown in tab.1. The specific coordinate information of 15 monitoring points inside the kiln body is shown in tab.2.

Table 1. Main technical parameters of hot air drying kiln

Parameters [mm]	Numerical value
Kiln Body (Length×Width×Height)	2500×1200×1500
Axial Fan (length×width×thickness)	500×500×300
Flat Shelf (Length×Width×Height)	2000×1200×50
Zone A (Length×Width×Height)	2500×1200×700
Zone B (Length×Width×Height)	250×1200×800
Zone C (Length×Width×Height)	2000×1200×750
Zone D (Length×Width×Height)	250×1200×800
Air Outlet (Length×Width×Height)	300×300×50

Table 2. Monitoring point coordinate information

Detection points	Coordinates X, Y, Z [mm]	Detection points	Coordinates X, Y, Z [mm]	Detection points	Coordinates X, Y, Z [mm]
B1	600,700,50	C7	600,1350,1250	D1	600,700,2300
B2	600,700,100	C6	600,1270,1250	D2	600,700,2350
B3	600,700,150	C5	600,1190,1250	D3	600,700,2400
B4	600,700,200	C4	600,1110,1250	D4	600,700,2450
/	/	C3	600,1030,1250	/	/
/	/	C2	600,950,1250	/	/
/	/	C1	600,870,1250	/	/

2.2 Experimental Data Collection Equipment and Methods

The experimental data acquisition equipment of the drying kiln is shown in Fig. 2. Online split plug-in anemometer model: VS110-D-500-S-II-A-1. The VS110 host is a standard plug-in sensor with a medium temperature of -40 to 150 degrees. The distributed online measurement method is used to obtain the wind speed data in the kiln.

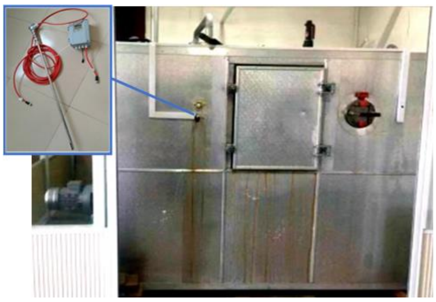

Figure 2.The experimental data acquisition equipment of the drying kiln

2.3 Boundary Condition Setting and Grid Division

The three-dimensional computational domain model of a hot air drying kiln is established by SpaceClaim. The structured grid is selected as the meshing method, and the hexahedral grid is selected as the grid form. The specific boundary layer setting is shown in tab. 3.

Table 3. Boundary condition setting

Setting items	Description
Fluid type	air
Turbulent flow model	standard k-ε model
Velocity Inlet	3m/s
Velocity outlet	outflow
Wall type	wall
Number of boundary layers	5
wall boundary conditions	no slip condition
Algorithm	SIMPLE

The 3-D model was meshed using ICEM CFD software (Grid density can affect calculation speed, and a small number of grids can result in significant errors in the calculation results. The solution results of the scheme with a total number of verified grids of approximately 1.56 million have grid independence). The results are shown in Fig. 3(a). Because during the drying operation, the temperature, humidity, and pressure of the drying medium inside the kiln are controlled, and the medium density is considered constant, velocity and vorticity are selected as the main parameters for analyzing the uneven distribution of the flow field. The corresponding numerical simulation results for velocity and vorticity in FLUENT are represented by velocity contour maps and streamline maps. After conducting numerical simulations in FLUENT, velocity contour maps and streamline maps for the current scheme S_0 of the hot air drying kiln are obtained, as shown in fig.3(b) respectively. Simulation data collected from CFD-Post was compared and analyzed against actual measurements inside the kiln. The results are shown in Fig. 3(c). The comparative results indicate that the trends of the simulated data are consistent with the measured data, and the relative errors are relatively small.

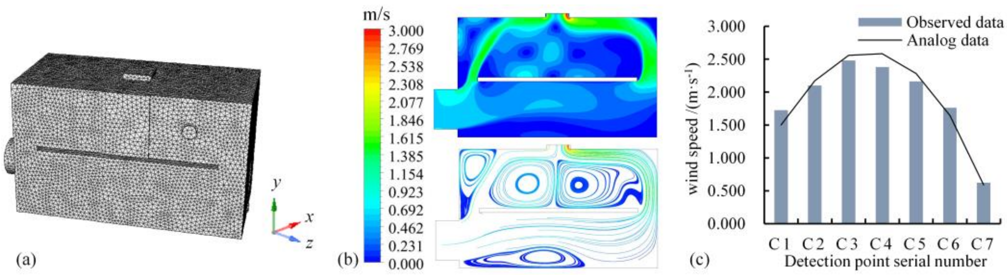

Figure 3. Numerical simulation results of the scheme S_0; (a)3-D Grid division results, (b)Velocity contour maps and Streamline maps, (c)Comparative analysis

It was found that there was a significant difference in airflow velocity between the left and right Axial Fan (air inlet) ducts in Zones B and D of the kiln, The difference between the two sample mean values of group B measured data and group D measured data is -1.872. Additionally, Zone C (material drying zone) exhibited an uneven distribution of wind speed flow field, The difference between monitoring points C1 and C7 is 0.916. Based on this, the initial problem for improvement was an uneven distribution of the wind speed flow field in Zone C of the hot air drying kiln. The improvement objective is to enhance the uniformity of wind speed flow field distribution in Zone C of the hot air drying kiln.

2.4 Mathematical Formulation

2.4.1 Control Equation

The flow control equations include the continuity equation, momentum equation, as well as turbulent kinetic energy transport and dissipation equations [13], as detailed below.

- The continuity equation：

$$\frac{\partial u_i}{\partial x_i}=0 \tag{1}$$

-The momentum equation：

$$\frac{\partial\left(\rho u_i u_j\right)}{\partial x_j}=-\frac{\partial P}{\partial x_j}+\frac{\partial}{\partial x_j}\left[\mu\left(\frac{\partial u_i}{\partial x_j}+\frac{\partial u_j}{\partial x_i}\right)\right]-\frac{2}{3}\frac{\partial}{\partial x_j}+\left(\mu\frac{\partial u_i}{\partial x_j}\right)+\rho g_i \tag{2}$$

Where u_i and u_j are the time-averaged velocities in the x_i and x_j directions, respectively. x_i is the three-axis coordinates of a cartesian coordinate system. μ is the air velocity inside the kiln. ρ calculates the air density inside the kiln. μ for dynamic viscosity. ρ is the air static pressure. g_i is the gravitational acceleration. x_i and x_j are the components of displacement in the i and j directions.

- Turbulent kinetic energy k and dissipation rate ε transport equations for are [14]：

$$\frac{\partial\left(\rho k u_i\right)}{\partial x_i}=\frac{\partial}{\partial x_j}\left[\left(\mu+\frac{u_i}{\sigma}\right)+\frac{\partial k}{\partial x_j}\right]+\mu_t\left(\frac{\partial u_i}{\partial x_j}+\frac{\partial u_j}{\partial x_i}\right)\frac{\partial u_i}{\partial x_j}-\rho\varepsilon \tag{3}$$

$$\begin{cases}\dfrac{\partial\left(\rho\varepsilon u_i\right)}{\partial x_i}=\dfrac{\partial}{\partial x_j}\left(\mu+\dfrac{u_i}{\sigma}+\dfrac{\partial\varepsilon}{\partial x_j}\right)+\rho c_1 E\varepsilon-\rho c_2\dfrac{\varepsilon^2}{k+\sqrt{v\varepsilon}}\\ E=\left(2E_{ij}E_{ji}\dfrac{1}{2}\right)\\ E_{ij}=\dfrac{1}{2}\left(\dfrac{\partial u_i}{\partial x_j}+\dfrac{\partial u_j}{\partial x_i}\right)\end{cases} \tag{4}$$

where μ_t is the turbulent viscosity. ν is kinematic viscosity. c_1=1.44, c_2=1.92, σ_k=1.0, σ_ε=1.2. E is the time-averaged strain tension, k is the turbulent Prandtl number of turbulent kinetic energy and ε is the turbulent Prandtl number of dissipation rate.

2.4.2 Scheme evaluation indicators and Numerical methods

This demonstrates the reliability of the model. To verify the feasibility of subsequent structural improvement schemes for the hot air drying kiln and to assess the changes in flow field uniformity in various numerical simulation scenarios, The visual comparison and analysis methods (velocity contour maps, streamline maps) and data comparison and analysis methods (velocity differences, overall mean velocity distribution, velocity unevenness coefficient) will be used. A total of 5 evaluation indicators [15-18] will serve as the basis for assessing the feasibility and rationality of the improvement schemes.

-Velocity contour maps

After conducting CFD numerical simulations on various improvement schemes, the color gamut distribution in the velocity contour maps of the numerical simulation results can intuitively observe the distribution of the wind speed flow field for each scheme.

-Streamline maps

After conducting CFD numerical simulations on various improvement schemes, the number of turbulence in each scheme's streamline maps can be observed intuitively through the streamline maps. In theory, the less turbulence there is inside the hot air drying kiln, the better.

-The overall mean of velocity distribution

The larger the overall mean of the velocity distribution, the stronger the drying medium strength, which is more conducive to the flow and transportation in the inlet ducts on both sides and the material drying area.

$$\bar{V}_a = \frac{\sum V_n}{n} \tag{5}$$

where $\bar{V}_a$ is the overall mean of the velocity distrib*ution*. n is the selected number of monitoring points. V_n represents the speed of each monitoring point.

- Velocity differences

The velocity data at monitoring points in Zone C (material drying zone) for each improvement scheme are subtracted to calculate the differences. A smaller difference indicates that the velocity difference between the top and bottom of the region is smaller, indicating relatively better uniformit*y* in the velocity flow field.

$$\Delta V = V_1 - V_7 \tag{6}$$

where ΔV is the airflow velocity difference at the monitoring point; V_1 is the wind speed data of monitoring point 1. V_7 is the wind speed data of monitoring point 7.

- Velocity unevenness coefficient

To evaluate the uniformity of velocity distribution inside the kiln body, the velocity unevenness coefficient *M* is introduced, and the calculation formula is:

$$M = \frac{\sigma_V}{\bar{V}_a} \times 100\% \tag{7}$$

where σ_V is the standard deviation of speed. The larger the velocity unevenness coefficient M, the more uneven the internal wind speed flow field; The smaller the *M*, the better the uniformity of the wind speed flow field.

3. Results

3.1 Improvement Ideas of Optimization Scheme of Hot Air Drying Kiln

Based on the functional model tool in TRIZ, a functional analysis model is established for the initial problem [19,20], as shown in Fig. 4.

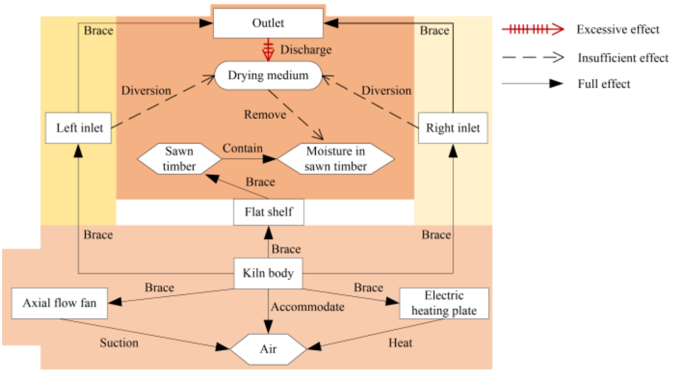

Figure 4. Function model of hot air drying kiln

According to fig.4, there are two reasons for the insufficient removal of moisture in sawn timber by the drying medium; The first is that the air outlet setting in the existing scheme (S_0) is unreasonable, resulting in the drying medium not effectively exchanging heat with the sawn timber and complete the function of removing moisture in the sawn timber. The second is that Zone B (left inlet) and Zone D (right inlet) have insufficient guiding effects on the drying medium, resulting in a large area of turbulence in the drying medium in Zone C (material drying zone). To solve these two problems, Optimization scheme Group 1 (Change the position of the outlet) and Optimization scheme Group 2 (Airflow distribution chamber with different parameter combinations) are established.

3.2 Comparative Analysis of Simulation Results of Specific Optimization Schemes

3.2.1 Optimization Scheme Group 1 (Change the Position of the Outlet)

Numerical simulations of the improvement scheme will be conducted using FLUENT, and the experimental results will be compared to obtain the optimal solution. To enhance the uniformity of the flow field in Zone C, the first consideration is to reduce the airflow velocity difference between the two sides of the Axial Fan (air inlet) ducts in Zones B and D to achieve the expected value of $\pm 0.200\ m \cdot s^{-1}$. Two schemes are proposed by adjusting the position parameters of the outlet (scheme S_1: placing the outlet at the near end of the axial flow fan, scheme S_2: placing the outlet at the far end of the axial flow fan). Fig.5 shows the visual comparative and analysis method used to compare and analyze scheme S_1 and the scheme S_2.

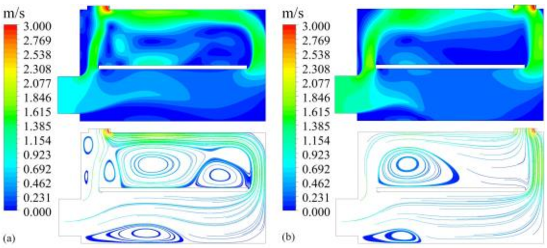

Figure 5. The visual comparison and analysis methods 1; (a) Scheme S_1, (b) Scheme S_2

After comparing and observing schemes (S_0, S_1, S_2) using visual comparison and analysis methods, it was found that the airflow velocity fields in Scheme S_2 were relatively more uniform, with the least turbulent flow. Furthermore, a comparative analysis of the data from 45 monitoring points in Zones B, C, and D for the three schemes was conducted (fig.6) . In Fig. 5, Scheme S_2 shows a relatively smooth distribution of monitoring points in Zones B and D compared to the other two schemes. Additionally, the velocity difference between the Axial Fan (air inlet) ducts in Zones B and D for Scheme S_2 is the smallest, meeting the expected value of $\pm 0.200\ m/s^{-1}$.

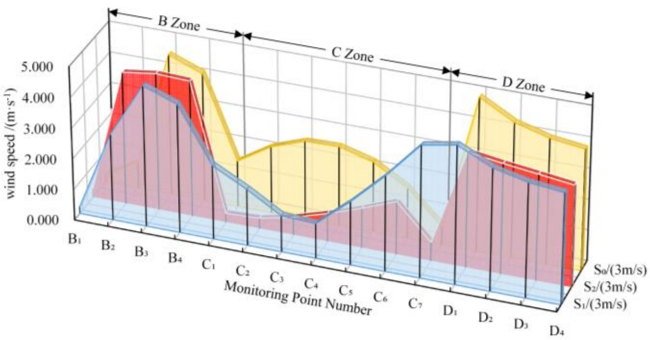

Figure 6.Comparison of monitoring point data between schemes S_1, S_2, and schemes S_0

By applying Eq. (5), (6), and (7) along with the wind speed data from monitoring points in Fig. 5, tab.4 is obtained by calculation.

Table 4. Data comparison between schemes S_1 , S_2 and schemes S_0

Scheme	The overall mean value of velocity distribution/[m·s^{-1}]	Velocity differences /[m·s^{-1}]	Velocity unevenness coefficient *M*
S_1	0.834	-0.311	0.585
S_2	2.141	-0.876	0.366
S_0	1.905	0.915	0.347

In tab.4, the overall mean value of velocity distribution for scheme S_2 is the highest at 2.141, which is an improvement of 12.39% compared to the S_0. This proves that the airflow velocity has been enhanced in scheme S_2. The velocity differences of scheme S_2 tend closer to 0 more than that of scheme S0, which proves that the airflow velocity field of scheme S_2 is relatively uniform. It was found that the velocity unevenness coefficient for Zone C in scheme S_2 is 0.366, which is higher than scheme S_0's velocity unevenness coefficient of 0.347. Therefore, further iterative optimization of the airflow velocity field in Zone C of scheme S_2 is still necessary.

Due to the relatively uniform airflow velocity field, minimal turbulence, highest overall mean velocity distribution, and achieving the expected velocity difference, this demonstrates that improving the outlet position to the far end is more conducive to enhancing the overall mean velocity distribution within the kiln and reducing the velocity difference between the Axial Fan (air inlet) ducts on both sides. scheme S_2 is deemed superior to scheme S_1 and scheme S_0 in the first round of improvement iterations and will serve as the basis for the second round of improvement iteration.

3.2.2 Optimization Scheme Group 2 (Airflow Distribution Chamber with Different Parameter Combinations)

By varying the parameters such as the number and aperture of the air distribution chamber vents, two types of airflow distribution chamber schemes, totaling six, have been designed for Zone B inside the kiln, aimed at optimizing the airflow velocity field in Zone C. Using FLUENT software, numerical simulations of the airflow velocity field were conducted for the above six airflow distribution chamber design schemes. Fig.6 shows the visual comparative and analysis method from scheme S_3 to scheme S_8.

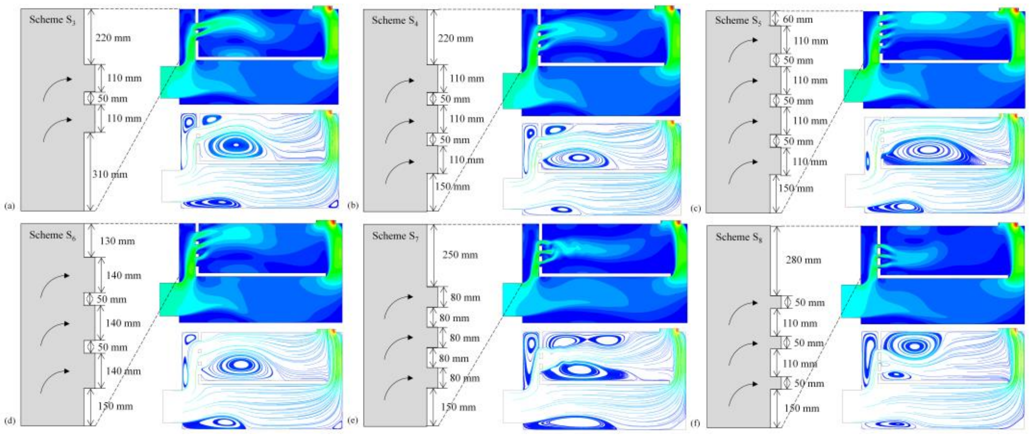

Figure 7. The visual comparison and analysis methods 2; (a)Scheme S_3, (b)Scheme S_4, (c)Scheme S_5, (d)Scheme S_6, (e)Scheme S_7, (f)Scheme S_8

The first type of design involves setting the vents of the airflow distribution chamber in a different number with, the same aperture configuration. Three schemes (S_3, S_4, S_5) have been designed accordingly, The numerical simulation results are illustrated in Fig. 7(a), Fig.7(b), and Fig. 7(c).

The second type of design involves setting the vents of the airflow distribution chamber in the same number, different aperture configuration. Three schemes (S_6, S_7, S_8) have been designed accordingly, The numerical simulation results are illustrated in Fig. 7(d), Fig.7(e), and Fig. 7(f).

Furthermore, applying Eq. (5), (6), and (7) to calculate the numerical values of monitoring points for schemes S_3 to S_8, and comparing them with scheme S_2, the results are shown in tab.5.

Table 5. Data comparison between schemes S_3 to S_8 and schemes S_2

Scheme	The overall mean value of velocity distribution/[m·s^{-1}]	Velocity differences /[m·s^{-1}]	Velocity unevenness coefficient *M*
S_3	1.287	-0.572	0.475
S_4	1.580	-0.316	0.363
S_5	1.144	-1.691	0.644
S_6	1.301	-1.379	0.445
S_7	1.208	0.031	0.656
S_8	1.004	-0.009	0.283
S_2	2.141	-0.876	0.366

From tab.5, it can be observed that scheme S_8 has the smallest velocity differences and velocity unevenness coefficient, performing the best in two out of the three evaluation indicators. Therefore, in the second round of improvement iteration, scheme S_8 is determined to be the optimal solution for optimizing the flow field in the hot air drying kiln.

3.3 Scheme Reliability Verification

In the actual wood drying process, the timber heat treatment typically involves several stages: the heating stage, the heat treatment stage, the cooling stage, and the moisture content adjustment stage (each requiring different flow velocities). To validate the reliability of scheme S_8 in the context of actual wood drying processes, numerical simulations were conducted for scheme S_8 under five different airflow conditions (standard airflow conditions: 3m/s, 5m/s, 7m/s; extreme airflow conditions: 1m/s, 9m/s). The monitoring point data in Zone C for scheme S_8 were compared with those of the scheme S_0 (fig.7).

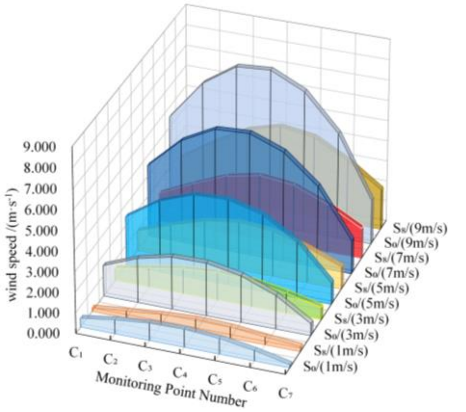

Figure 8. Comparison of monitoring data between the scheme S_0 and the scheme S_8

It can be observed that scheme S_8 exhibits consistent flow field patterns under the five different airflow conditions. Additionally, the variation range of the airflow velocity difference between the bottom monitoring point C1 and the top monitoring point C7 is smaller for scheme S_8 compared to scheme S_0. This demonstrates the reliability of its structural design.

Further applying Eq. (5), (6), and (7) to calculate the numerical values of various monitoring points for the scheme S_0 and scheme S_8 and comparing the data (3m/s,5m/s,7m/s), as shown in tab.6.

Table 6. Data comparison between the initial scheme S_0 and scheme S_8

Wind speed situation	Scheme	The overall mean value of velocity distribution/[m·s^{-1}]	Velocity differences /[m·s^{-1}]	Velocity unevenness coefficient M
3m/s	S_0	1.905	0.915	0.347
	S_8	1.004	-0.009	0.283
5m/s	S_0	3.115	1.382	0.335
	S_8	1.722	-0.081	0.289
7m/s	S_0	4.501	1.886	0.322
	S_8	2.398	-0.181	0.272

It can be observed from tab.6, scheme S_0 will cause the overall mean value of velocity distribution in Zone C in the kiln to be too high when the Axial Fan (air inlet) is 5m/s and 7m/s, which will more easily lead to the deformation of the sawn timber during drying. when scheme S_8 is under three different wind speeds situation, the overall mean value of velocity distribution is all in line with the ideal range of 1~3m/s, proving that the structural design of scheme S_8 can obtain reliability drying effect, the velocity differences and velocity unevenness coefficient of the scheme S_8 is all less than the scheme S_0, proving that the design has better stability of the wind speed and has an optimal uniformity of the wind speed flow field. When scheme S_0 and scheme S_8 have the same wind speed situation (3m/s), the velocity differences of scheme S_8 tend closer to 0 more than that of scheme S_0, and the velocity unevenness coefficient decreases by 18.44%. It can be concluded that scheme S_8 is superior to the scheme S_0.

4. **Conclusions**

This study focuses on the wood hot air drying kiln and addresses the issue of uneven airflow distribution within the kiln. Without adding baffle plates or altering the structure to incorporate right-angle surfaces, the kiln's structure was optimized by adjusting the position of the air outlet and installing airflow distribution chambers. Computational fluid dynamics (CFD) analysis using FLUENT software was conducted to evaluate the airflow distribution of the proposed improvements. The conclusions drawn from experimental validation are as follows:

- Changing the position of the air outlet has a certain effect on improving the uniformity of the airflow within the kiln. Comparing the design of placing the air outlet at the far end of the axial flow fan with the current scheme, the former results in a more uniform flow field within the kiln and a significant reduction in turbulent flow.
- The addition of an airflow homogenization chamber can effectively improve the flow field uniformity and reduce the occurrence of uneven flow field distribution.
- Scheme S_8 in the air supply speed of 3m/s to 7m/s, the kiln Zone C (material drying area) flow field to meet the ideal interval of 1~3m/s, and still maintain a better drying medium flow stability and uniformity of the kiln flow field distribution.

The study shows that it is feasible, reasonable, and effective to optimize the flow field in the kiln by improving the structural parameters of the drying kiln. However, because wood drying is a complex nonlinear process, and its hot air drying process is affected by many factors, it is difficult to fully simulate all the details and influencing factors in the actual drying process. The wood drying simulation experiment has certain limitations in the accuracy of the difference between the numerical simulation and the actual drying process, the boundary conditions, and the parameter settings. In future research, the influencing factors such as thermal conductivity and initial moisture content of wood will be gradually increased, and the accuracy of simulation results will be gradually improved by adjusting boundary conditions and parameter settings. In the subsequent improvement process, the feasibility of the structural improvement scheme of the hot air drying kiln will be verified by the actual measurement method.

Nomenclature

u - Air velocity inside the kiln，[$m\cdot s^{-1}$，m/s]

ρ - Air density inside the kiln，[kg/m^3]

μ -Dynamic viscosity，[Pa·s]

P -Air static pressure，[Pa]

g_i - Gravitational acceleration，[$kg/(m\cdot s)^2$]

μ_t - Turbulent viscosity，[Pa/s]

ν - Kinematic viscosity，[m^2/s]

References

[1] Zhao, J. Y., Cai, Y. *C.*, A comprehensive mathematical model of heat and moisture transfer for wood convective drying, *Holzforschung*, *71*(2017),5,pp.425-435

[2] Geng Z. H., *et al.*, Research on drying uniformity and technology of sea buckthorn with infrared combined hot air based on temperature and humidity control, *Transactions of the Chinese Society of Agricultural Engineering (Transactions of the CSAE), 1-17*[2023-11-13]. https://kns-cnki-net.webvpn.nefu.edu.cn/kcms/detail/11.2047.S.20230927.1010.002.html.

[3] Carrera Escobedo, J. L., *et al.*, Computational fluid dynamics analysis for improving temperature distribution in a chili dryer, *Thermal Science,22*(2018),6,pp.2615-2623

[4] Coban, S. O., *et al.*, A review on computational fluid dynamics simulation methods for different convective drying applications, *Thermal Science,27*(2023),1B,pp.825-842

[5] Kadem, S., *et al.*, Computational analysis of heat and mass transfer during microwave drying of timber, *Thermal Science,20*(2016),5,pp.1447-1455

[6] Mecha, P., *et al.*,Deflectors As The Performance Booster Component In Designing A Side-Ventilated Heat Pump Cabinet Dryer For Vegetables, *Thermal Science*,*27*(2023),6B,pp.4989-5004

[7] Marković, Z. J., *et al.*,Numerical simulation of the gas flow through the rectangular channel with perforated plate, *Thermal Science*,*27*(2023),3B,pp.2241-2253

[8] Chen Z. F., *et al.*, Numerical simulation and experiment of four-way ventilation mixed flow drying section for rice. *Transactions of the Chinese Society of Agricultural Engineering (Transactions of the CSAE),38*(2022), 24,pp.237-247

[9] Chen Z .J., *et al.*, Air supply velocity and temperature optimization of hot air drying room based on forced convection. *Transactions of the Chinese Society of Agricultural Engineering (Transactions of the CSAE),38*(2022), S1,pp.37-46

[10] Lan L. X., *et al.*, Newly advances in wood science and technology. *Transactions of the Chinese Society for Agricultural Machinery*,1-8[2023-11-13].https://kns-cnki-net.webvpn.nefu.edu.cn/kcm

s/detail/11.1964.S.20230925.0852.006.html.

[11] Wang Z. W., *et al.*, Optimal simulation design of structure and parameter in heat pump drying room. *Transactions of the Chinese Society for Agricultural Machinery,51*(2020), S,pp.464-475

[12] Elustondo, D., *et al.*, Advances in wood drying research and development, *Drying Technology,41*(2023),6,pp.890-914

[13] Yu H. M., *et al.*, Optimization Design and Performance Test of Multi-layer Tray Straw Tray Hot Air Assisted Microwave Drying Device. *Transactions of the Chinese Society for Agricultural Machinery*, 1-23[2023-11-13].https://kns-cnki-net.webvpn.nefu.edu.cn/kcms/detail/11.1964.S.20230921.0923.002.html.

[14] Zhu Y. F., *et al.*, Influence of improved structure of drying kiln on the uniformity of wind velocity flow field. *Transactions of the Chinese Society of Agricultural Engineering,37*(2021),24,pp.327-337.

[15] Dong L., *et al.*, Flow Field Simulation and Structural Optimization of Mesh-Belt Pepper Drying Machine. *Transactions of the Chinese Society for Agricultural Machinery*, 1-9[2023-11-14].https://link.cnki.net/urlid/11.1964.s.20230925.1019.018

[16] Menasria F., *et al.*, Numerical study of thermohydraulic performance of solar air heater duct equipped with novel continuous rectangular baffles with high aspect ratio. *Energy, 133*(2017),X,pp.593-608.

[17] Liu H., *et al.*, Influence of air distribution plate on flow characteristics of nonhomogeneous particles in shallow fluidized-bed with immersed pipes. *The Chinese Journal of Process Engineering,23*(2023),2,pp.216-225

[18] Jiang D. L., *et al.*, Desing and Performance Verification of Infrared Combined Hot Air Drying Device. *Transactions of the Chinese Society for Agricultural Machinery,53*(2022),12,pp.411-420

[29] Meng Y., Dinçer H., Yüksel S., TRIZ-Based Green Energy Project Evaluation Using Innovation Life Cycle and Fuzzy *Modeling. IEEE Access,9*(2021),X,pp.69609-69625

[20] Zheng J., *et al.*, Design of the integrated precision pneumatic seed metering device for rapeseed using TRIZ-AD. *Transactions of the Chinese Society of Agricultural Engineering,39*(2023),14,pp.49-59

Submitted: 08.04.2024.

Revised: 04.06.2024.

Accepted: 26.06.2024